Journal of Solid State Chemistry 187 (2012) 186–194

Contents lists available at SciVerse ScienceDirect

Journal of Solid State Chemistry

journal homepage: www.elsevier.com/locate/jssc

Structural and electronic properties of $Sr_xBa_{1-x}SnO_3$ from first principles calculations

E. Moreira [a], J.M. Henriques [b], D.L. Azevedo [c], E.W.S. Caetano [d,*], V.N. Freire [e], E.L. Albuquerque [f]

[a] Departamento de Física Teórica e Experimental, Universidade Federal do Rio Grande do Norte, 59072-970 Natal-RN, Brazil
[b] Centro de Educação e Saúde, Universidade Federal de Campina Grande, Campus Cuité, 58175-000 Cuité-PB, Brazil
[c] Departamento de Física, Universidade Federal do Maranhão, Centro de Ciências Exatas e Tecnologia, 65085-580 São Luís-MA, Brazil
[d] Instituto Federal de Educação, Ciência e Tecnologia do Ceará, 60040-531 Fortaleza-CE, Brazil
[e] Departamento de Física, Universidade Federal do Ceará, Centro de Ciências, Caixa Postal 6030, Campus do Pici, 60455-760 Fortaleza-CE, Brazil
[f] Departamento de Biofísica e Farmacologia, Universidade Federal do Rio Grande do Norte, 59072-970 Natal-RN, Brazil

ARTICLE INFO

Article history:
Received 5 August 2011
Received in revised form
16 December 2011
Accepted 23 December 2011
Available online 4 January 2012

Keywords:
$Sr_xBa_{1-x}SnO_3$
DFT calculations
Structural properties
Band structure
Effective masses

ABSTRACT

Neutron diffraction data for $Sr_xBa_{1-x}SnO_3$ ($x=0.0$, 0.2, 0.4, 0.6, 0.8 and 1.0) solid solutions were used as inputs to obtain optimized geometries and electronic properties using the density functional theory (DFT) formalism considering both the local density and generalized gradient approximations, LDA and GGA, respectively. The crystal structures and SnO_6 octahedra tilting angles found after total energy minimization agree well with experiment, specially for the GGA data. Elastic constants were also obtained and compared with theoretical and experimental results for cubic $BaSnO_3$. While the alloys with cubic unit cell have an indirect band gap, tetragonal and orthorhombic alloys exhibit direct band gaps (exception made to $x=1.0$). The Kohn–Sham minimum electronic band gap oscillates from 1.52 eV (cubic $x=0.0$, LDA) to 2.61 eV (orthorhombic $x=1.0$, LDA), and from 0.74 eV (cubic $BaSnO_3$, GGA) to 1.97 eV (orthorhombic $SrSnO_3$, GGA). Parabolic interpolation of bands has allowed us to estimate the effective masses for charge carriers, which are shown to be anisotropic and larger for holes.

1. Introduction

$Sr_xBa_{1-x}SnO_3$ and $Sr_xCa_{1-x}SnO_3$ are alloys of perovskite-type earth stannates, $ASnO_3$ (A=Ba, Sr, Ca), an important class of materials having unusual properties like ferroelectricity, ferromagnetism and superconductivity [1], which is used for antistatic coatings, photovoltaic cells, electroluminescent flat displays and optoelectronic devices [2]. In particular, the compounds $CaSnO_3$ and $SrSnO_3$ are basic structures for development of dielectric materials for capacitors, lithium batteries and humidity sensors [3]. $Sr_xBa_{1-x}SnO_3$ and $Sr_xCa_{1-x}SnO_3$ samples can be prepared by mixing stoichiometric quantities of $BaCO_3$, $SrCO_3$, $CaCO_3$ and SnO_2 to form pellets, which are pressed under a load of 9 tons and fired at about 1400 °C for 24 h. After cooling these solid state samples to room temperature, neutron diffraction data shows the existence of a single perovskite phase with SnO_6 octahedra that tilt about the symmetry axes [4]. While all the $Sr_xCa_{1-x}SnO_3$ samples have the *Pbnm* superstructure, the alloy $Sr_xBa_{1-x}SnO_3$ has the *Pbnm* superstructure with $x=1.0$ ($SrSnO_3$) and $x=0.8$, another orthorhombic structure with space group *Imma* for $x=0.6$, a tetragonal *I4/mcm* phase with $x=0.4$, and an undistorted cubic $Pm\bar{3}m$ structure with $x=0.2$ and $x=0.0$ ($BaSnO_3$) [4].

Considering the technological and the theoretical interest on earth stannates, an electronic structure study for $CaSnO_3$ ilmenite was performed using the linear muffin-tin orbital method and the atomic sphere approximation including the combined correction [5]. The Perdew–Wang generalized gradient approximation (GGA) was employed to treat the effects of exchange and correlation. A 4.0 eV direct energy gap was obtained for ilmenite $CaSnO_3$, which is in good agreement with the measured value of 4.4 eV [5]. Density functional theory (DFT) first principles calculations of the structural parameters, electronic structure, carriers' effective masses, and optical absorption of orthorhombic $CaSnO_3$ were performed within the local density and generalized gradient approximations, LDA and GGA, respectively [6]. A good agreement between the calculated lattice parameters and experimental results was obtained, and a direct energy gap of 1.95 eV (2.92 eV) was estimated in the GGA (LDA) for orthorhombic $CaSnO_3$. Small effective masses were estimated, with electron effective masses practically isotropic, allowing one to infer that direct gap orthorhombic $CaSnO_3$ is a semiconductor with potential for optoelectronic applications [6].

On the other hand, the $SrSnO_3$ cubic phase was studied within the framework of the local density functional approximation using the full-potential linearized augmented plane wave

* Corresponding author. Fax: +55 85 3307 3711.
E-mail address: ewcaetano@gmail.com (E.W.S. Caetano).

0022-4596/$ - see front matter © 2012 Elsevier Inc. All rights reserved.
doi:10.1016/j.jssc.2011.12.027

(FLAPW) method [7], being demonstrated that it is a semiconductor with an indirect band gap (R and M $\rightarrow\Gamma$) of $\approx$ 1.03 eV [8]. Bannikov et al. [7] using the same calculation method found a direct band gap of 0.95 eV for the $SrSnO_3$ cubic phase. Band structure calculations employing the density-functional theory formalism within the GGA approximation, as well as ultraviolet diffuse reflectance and photoluminescence spectroscopy were employed to assess the emission mechanism of orthorhombic $SrSnO_3$ [9]. According to these authors, the calculated band gap to orthorhombic $SrSnO_3$ was 1.8 eV. Experimental and computational studies on the electronic structure of ternary oxides performed for the orthorhombic $SrSnO_3$ with ultraviolet diffuse reflectance and the linear muffin-tin orbital (LMTO) method obtained an experimental (calculated) energy band gap of 4.1 eV (2.5 eV) [2]. Recently, orthorhombic $SrSnO_3$ was investigated using both the LDA and GGA approaches, the electronic band structure, density of states, dielectric function and optical absorption being evaluated, as well as the infrared and Raman spectra, in good agreement with experiment, after computing the vibrational modes of the crystals at $\mathbf{q}=0$ [10]. Dielectric optical permittivities and polarisabilities at $\omega=0$ and $\omega=\infty$ were calculated as well. An indirect band gap E(S $\rightarrow\Gamma$)=1.97 eV (2.27 eV) was obtained within the GGA (LDA) level of calculation. Effective masses for holes and electrons were estimated to be very anisotropic comparing with those of orthorhombic $CaSnO_3$. In the energy range between 3.0 eV and 7 eV, approximately, the optical absorption of orthorhombic $SrSnO_3$ increases slowly. Starting from 7.3 eV to larger energies, however, the optical absorption increases faster due to the appearance of transitions involving mainly O 2p valence states and Sn 5 s conduction states.

In this work, the structural and electronic properties of the alloy $Sr_xBa_{1-x}SnO_3$ with x=0.0, 0.2, 0.4, 0.6, 0.8 were calculated using LDA and GGA exchange-correlation functionals using the virtual crystal approximation (VCA), which is known to be a simple and efficient approach to describe alloys [11], having been employed to study doping and disorder effects in Si/Al compounds [12,13], nitridosilicates and oxonitridoaluminosilicate systems [14], and perovskite solid solutions [11]. The neutron diffraction data for $Sr_xBa_{1-x}SnO_3$ powder of Mountstevens et al. [4] were used to prepare the inputs for the numerical calculations. The converged unit cell of each alloy was obtained, from which the electronic band structure, electronic density of states, energy band gaps and carrier effective masses along the most important high symmetry directions were calculated. An almost linear and a smooth parabolic increase (from 0.74 eV for cubic $BaSnO_3$ to 1.97 eV for orthorhombic $SrSnO_3$), respectively, of the SnO_6 octahedra tilting and DFT-GGA calculated energy band gap with the alloy Sr content x were obtained, notwithstanding the distinct unit cell symmetries of the alloys.

2. Methodology

All calculations were performed using the crystallographic data obtained from Mountstevens et al. [4], the electronic properties of $Sr_xBa_{1-x}SnO_3$ (x=0.0, 0.2, 0.4, 0.6, 0.8, 1.0) being performed within the density functional theory [15,16] (DFT) approach. The x=0.2 crystal has the undistorted cubic perovskite structure with space group $Pm\bar{3}m$ (see Fig. 1(a)). For x=0.4, a tetragonal structure with space group $I4/mcm$ is reported, exhibiting a tilting of SnO_6 octahedra about the c-axis (Fig. 1(b)). The x=0.6 orthorhombic crystal belongs to the *Imma* space group with the tilting of SnO_6 octahedra about the diad axis parallel to the b-axis (as shown in Fig. 2(a)). Finally, the x=0.8 alloy has an orthorhombic structure with space group *Pbnm*, displaying a tilting of SnO_6 octahedra about the c-axis and tilting about the diad axis parallel to the b-axis (Fig. 2(b)).

In order to carry out the computations we have chosen the CASTEP code [17]. Two exchange-correlation functionals were taken into account: the total local-density approximation (LDA) [16,18,19] and the generalized gradient approximation (GGA) [20,21]. The LDA functional follows a standard parametrization [22,23], while the GGA functional was the one proposed by Perdew–Burke–Ernzerhof [24], which produces results close to the obtained using the PW91 functional [25]. We have also adopted norm-conserving pseudopotentials [26] to replace the core electrons in each atomic species, all of them generated using the OPIUM code [27]. The electronic valence configurations for each atomic species were: Sr-$4s^24p^65s^2$, Ba-$5s^25p^66s^2$, Sn-$5s^25p^2$, and O-$2s^22p^4$ within the VCA approximation implemented in the CASTEP code [11,14]. VCA calculations use weights according with the site occupancies to obtain the contribution of each pseudopotential. As Sr and Ba have 10 valence electrons each, we could vary the Sr molar fraction x from 0.0 to 1.0 in steps of 0.2 maintaining an integer number of electrons per unit cell. A Monkhorst–Pack [28] sampling was used to evaluate all integrals in reciprocal space, its grid being selected to ensure a well converged electronic structure for each crystal.

Lattice parameters and atomic positions were optimized by seeking a total minimum energy for the $Sr_xBa_{1-x}SnO_3$ (x = 0.0,0.2, 0.4,0.6,0.8,1.0) unit cell. The convergence tolerances for all geometry optimizations were: total energy change smaller than 0.5×10^{-5} eV/atom, maximum force per atom below 0.01 eV/Å, pressure smaller than 0.02 GPa, and maximum atomic displacement not exceeding 0.5×10^{-3} Å. The convergence tolerance window was of two successive steps, and the optimization method used the BFGS minimizer [29]. Within each self-consistent field (SCF) step, the electronic minimization parameters for convergence were: total energy/atom smaller 0.5×10^{-6} eV, electronic eigenenergy variation smaller than 0.1235×10^{-6} eV at most, and a convergence window of three SCF cycles. A plane-wave basis set was adopted to represent the Kohn–Sham orbitals, with cutoff energy chosen, after convergence studies, to be 800 eV. The quality of this basis set was kept fixed even taking into account the unit cell volume variations during the geometry optimization process.

Fig. 3 shows the unit cell total energy variation (ΔE) as a function of the unit cell volume (V) relative to the optimized volume (V_0). In order to plot the curves, we have carried out single point energy calculations for enlarged (reduced) unit cells, where the enlargement (reduction) was achieved by multiplying the lattice parameters of the optimized structure always by the same factor, fixing the fractionary atomic coordinates. As one can see, the ΔE curves are approximately parabolic, with pairs of very similar curves corresponding to the molar fractions x=0.0 and 0.2 (approximate parabolas with smoother curvature, cubic structures), x=0.4 and 0.6 (approximate parabolas with intermediate curvature, tetragonal and orthorhombic alloys, respectively), and x=0.8 and 1.0 (approximate parabolas with more pronounced curvature, orthorhombic structures).

After obtaining the optimized unit cells and atomic positions, the Kohn–Sham electronic band structure and the partial density of states (PDOS) were evaluated for both the optimized LDA and GGA unit cells. Effective masses at the extreme of the valence and conduction bands were also estimated by quadratic interpolation of the corresponding band curves [30–34].

3. Results and discussion

3.1. Geometry optimization

In Table 1 one can see the computed lattice parameters and unit cell volumes for $Sr_xBa_{1-x}SnO_3$, as well as the experimental

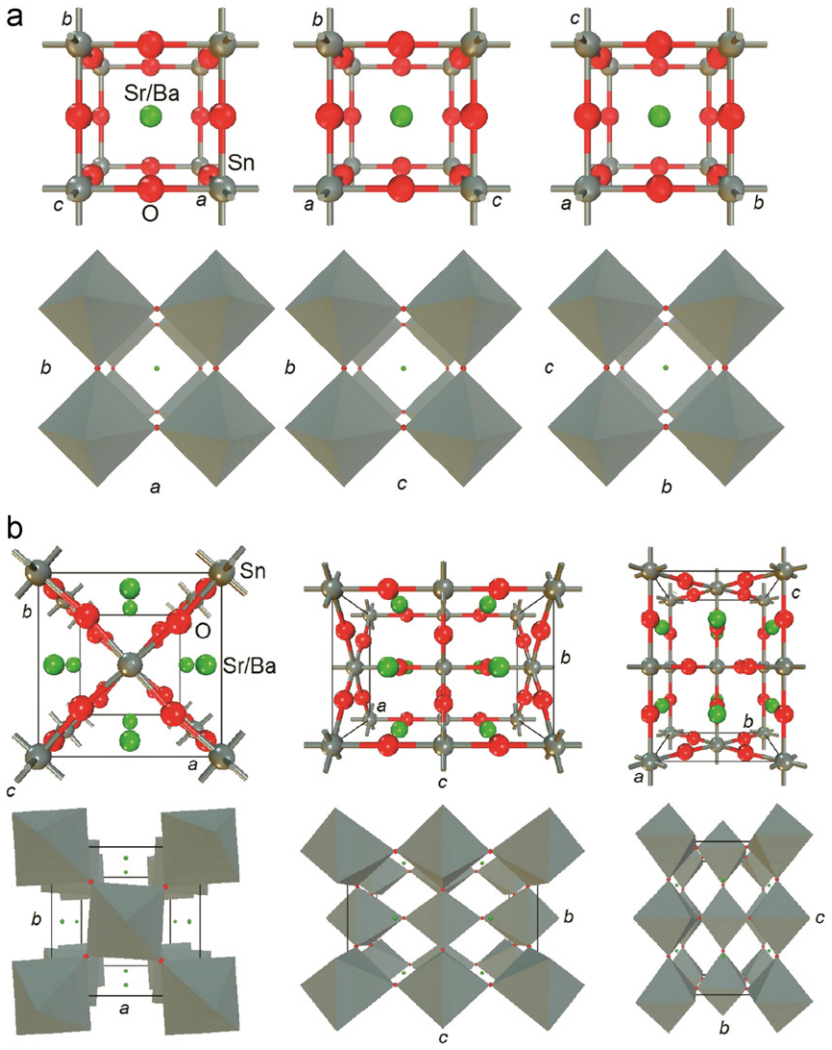

Fig. 1. (a) Crystal structure of $Sr_{0.2}Ba_{0.8}SnO_3$ cubic. Top: different views of the unit cell and atomic labels. Bottom: tilted SnO_6 octahedra in the cubic $Sr_{0.2}Ba_{0.8}SnO_3$ unit cell. (b) Crystal structure of $Sr_{0.4}Ba_{0.6}SnO_3$ tetragonal. Top: different views of the unit cell and atomic labels. Bottom: tilted SnO_6 octahedra in the tetragonal $Sr_{0.4}Ba_{0.6}SnO_3$ unit cell.

values from Ref. [4]. Fractionary atomic coordinates for $Sr_xBa_{1-x}SnO_3$ are shown in Table 2. LDA lattice parameters are smaller due to the well-known trend of this functional to overestimate the strength of interatomic interactions. For cubic $Sr_{0.2}Ba_{0.8}SnO_3$, the relative difference between the a values of LDA and experiment is -1.7% and the predicted unit cell volume is smaller by 5.0%; for tetragonal $Sr_{0.4}Ba_{0.6}SnO_3$ the largest difference between LDA and experimental lattice parameters is also about -1.7% and unit cell volume is smaller by 5.1%; for orthorhombic $x=0.6$ the worst case is the a parameter (-1.9% compared with experiment), while the unit cell volume is smaller by 5.1%; for orthorhombic $Sr_{0.8}Ba_{0.2}SnO_3$, LDA predicts a b parameter 2.0% smaller than the experimental value and an unit cell volume reduced by 5.1%. The GGA exchange-correlation functionals, on the other hand, tend to underestimate the strength of interatomic forces, leading to larger lattice parameters [20,21]. In comparison with the LDA results, the GGA estimates for $Sr_xBa_{1-x}SnO_3$ show the best agreement with neutron diffraction data. For cubic $Sr_{0.2}Ba_{0.8}SnO_3$, the GGA lengths for the lattice parameters are larger than experimental lengths by 0.6% at most and the predicted GGA unit cell volume is $+1.9\%$ larger than the experimental value. For tetragonal $Sr_{0.4}Ba_{0.6}SnO_3$, the GGA results show a larger unit cell with relative differences between $+0.4\%$ (a and b) and $+0.9\%$ (c), and the unit cell volume is larger by $+1.8\%$. For orthorhombic $Sr_{0.6}Ba_{0.4}SnO_3$, the b lattice parameter is larger by $+0.7\%$ and the unit cell volume is larger by $+1.9\%$. For orthorhombic $Sr_{0.8}Ba_{0.2}SnO_3$, the GGA results predict a larger unit cell with differences between $+0.4\%$ (b) and $+0.7\%$ (a and c), and the unit cell volume is larger by $+1.9\%$ in comparison with the measured data.

The variation of the structural parameters of $ASnO_3$ crystals (A=Ba, Sr, Ca) and their alloys with increasing A cation radius has been studied by Mountstevens et al. [4], showing a direct correlation between the unit cell volume with increasing A cation size. The alkaline earth stannates at 300 K have the following crystal structure symmetries with increasing A cation radius: $Pbnm \rightarrow Imma \rightarrow I4/mcm \rightarrow Pm\bar{3}m$. This sequence of transitions is also seen at high temperatures in $SrZrO_3$ [35] and in $SrRuO_3$ [36]. The tilting of the SnO_6 octahedra in perovskite structures can be calculated from structural parameters with the method proposed by Kennedy et al. [36] using the O2 fractionary atomic positions in the *Pbnm*, *Imma* and *I4/mcm* unit cells. The tilting of octahedra in adjacent unit cells can occur in the same sense (in-phase tilting, ϕ^+) or in the opposite sense (out-of-phase tilting, ϕ^-), thus we have plotted both tilting angles in Fig. 4 for the LDA, GGA and experimental data. As one can see, the tilting is 0 for the $x=0$ and $x=0.2$ (cubic structures), as expected, while the in-phase tilting angle is 0 for the crystals with $x=0.4,0.6$ (tetragonal and

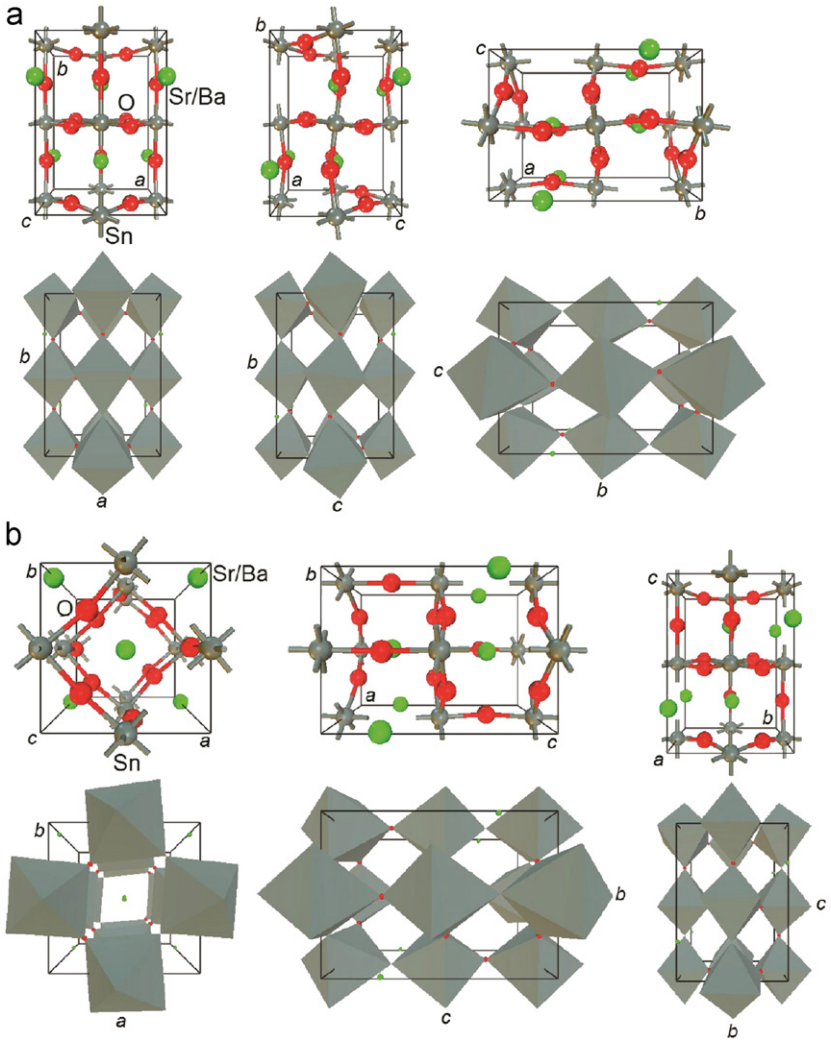

Fig. 2. (a) Crystal structure of $Sr_{0.6}Ba_{0.4}SnO_3$ orthorhombic. Top: different views of the unit cell and atomic labels. Bottom: tilted SnO_6 octahedra in the orthorhombic $Sr_{0.6}Ba_{0.4}SnO_3$ unit cell. (b) Crystal structure of $Sr_{0.8}Ba_{0.2}SnO_3$ orthorhombic. Top: different views of the unit cell and atomic labels. Bottom: tilted SnO_6 octahedra in the orthorhombic $Sr_{0.8}Ba_{0.2}SnO_3$ unit cell.

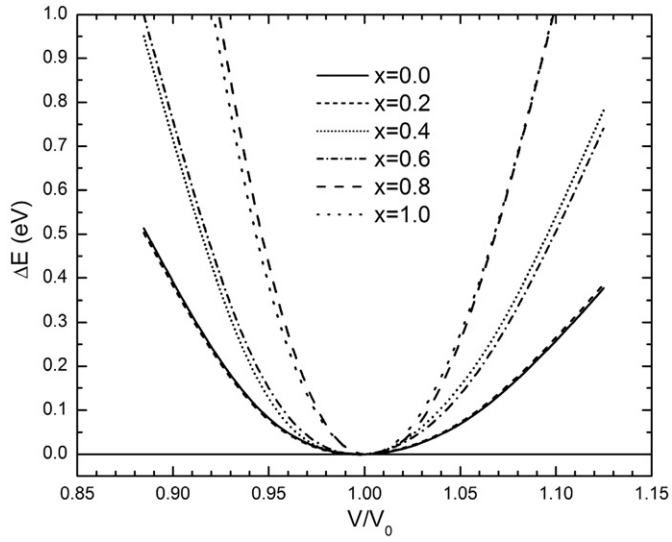

Fig. 3. $Sr_xBa_{1-x}SnO_3$ unit cell DFT total energy variation (ΔE) as a function of the volume of the unit cell (V) relative to the optimal volume (V_0) using the GGA-PBE functional.

orthorhombic, respectively). For x between 0.4 and 1.0, the experimental out-of-phase angle ϕ^- increases from 3.43° (x=0.4) up to 10.8° (x=1.0), while the LDA values vary from 3.66° to 10.9° in the same range, and the GGA values vary from 3.66° to 11.0°. So there is a nice agreement between the DFT computations and the neutron diffraction data when the ϕ^- is considered. In the case of the in-phase angle, we also observe a high degree of similitude between the theoretical and experimental data. For x=0.8, ϕ^+ is 9.67° in measurements and 8.54° (9.11°) in the LDA (GGA) estimations. All in all, the GGA predictions tend to be closer to the experimental values as we switch from one x value to another.

Using the GGA-PBE data, the top part of Fig. 5 shows, as a function of x, the variation of nine elastic constants: C_{11}, C_{22}, C_{33}, C_{44}, C_{55}, C_{66}, C_{12}, C_{13}, and C_{23}, while the bottom part depicts the bulk modulus (BM) and the Young modulus along x (Y_x), y (Y_y), and z (Y_z) at zero pressure. For $BaSnO_3$, the calculated value of BM was 139 GPa, close to previous theoretical calculations (144.0 GPa [38], 132 GPa [39]) and experimental results (145.8 GPa [40]). The C_{11}, C_{12}, and C_{44} elastic constants of $BaSnO_3$ we obtained were 251 GPa, 82.3 GPa, and 98.1 GPa, respectively, while the corresponding values calculated by Bouhemadou et al. [38] were 285.2 GPa, 68.5 GPa, and 84.3 GPa, in the same order. The

Table 1
Lattice parameters for $Sr_xBa_{1-x}SnO_3$ after DFT-LDA and GGA computations. Experimental data for $Sr_xBa_{1-x}SnO_3$ are also presented [4]. Lengths (a, b, c) are in Å and volumes (V) in Å^3.

Alloy/Data source	a	b	c	V
$BaSnO_3$				
LDA	4.045 (−1.7%)	4.045 (−1.7%)	4.045 (−1.7%)	66.18 (−5.0%)
GGA	4.142 (+0.6%)	4.142 (+0.6%)	4.142 (+0.6%)	71.08 (+2.0%)
Exp.	4.1151 (1)	4.1151 (1)	4.1151 (1)	69.69
$Sr_{0.2}Ba_{0.8}SnO_3$				
LDA	4.032 (−1.7%)	4.032 (−1.7%)	4.032 (−1.7%)	65.531 (−5.1%)
GGA	4.129 (+0.6%)	4.129 (+0.6%)	4.129 (+0.6%)	70.378 (+2.0%)
Exp.	4.102	4.102	4.102	69.022
$Sr_{0.4}Ba_{0.6}SnO_3$				
LDA	5.676 (−1.7%)	5.676 (−1.7%)	8.049 (−1.7%)	259.267 (−5.1%)
GGA	5.803 (+0.4%)	5.803 (+0.4%)	8.264 (+0.9%)	278.310 (+1.8%)
Exp.	5.777	5.777	8.187	273.231
$Sr_{0.6}Ba_{0.4}SnO_3$				
LDA	5.651 (−1.9%)	7.980 (−1.7%)	5.681 (−1.5%)	256.166 (−5.0%)
GGA	5.793 (+0.6%)	8.180 (+0.7%)	5.805 (+0.6%)	275.127 (+1.9%)
Exp.	5.758	8.121	5.767	269.669
$Sr_{0.8}Ba_{0.2}SnO_3$				
LDA	5.649 (−1.6%)	5.614 (−2.0%)	7.964 (−1.6%)	252.579 (−5.1%)
GGA	5.784 (+0.7%)	5.755 (+0.4%)	8.149 (+0.7%)	271.311 (+1.9%)
Exp.	5.741	5.728	8.091	266.068
$SrSnO_3$				
LDA	5.603 (−1.8%)	5.603 (−1.8%)	7.916 (−1.9%)	248.560 (−5.3%)
GGA	5.736 (+0.5%)	5.742 (+0.7%)	8.107 (+0.5%)	267.067 (+1.7%)
Exp. [37]	5.7082 (3)	5.7035 (3)	8.0659 (6)	262.600

differences between our results and theirs are probably due to the use of different types of pseudopotentials (we adopted norm-conserved pseudopotentials while Bohemadou and its coworkers preferred ultrasoft pseudopotentials, which allow for a smaller value of the plane-wave basis set cutoff energy). Farfán et al. [39], on the other hand, have chosen a full-potential (linearized) augmented plane-wave + local orbital method, including explicitly all electrons with relativistic effects, finding a bulk modulus 7 GPa smaller than our computed estimate. Shein et al. [41] have calculated the bulk modulus for cubic $SrSnO_3$ as 164.07 GPa using the same GGA-PBE exchange-correlation functional we used in this work. In comparison, we predict a bulk modulus of 141 GPa for orthorhombic $SrSnO_3$. We have not found in the literature any data on the elastic constants for the $Sr_xBa_{1-x}SnO_3$ alloys with x between 0.2 and 0.8.

As the Sr x molar fraction increases from 0.0 to 1.0, we note (see Fig. 5, top) that the C_{11} and C_{22} elastic constants change by a small amount, while the C_{33} constant varies in a more pronounced way, from 251 GPa at $x=0.0$ down to 226 GPa for $x=0.8$. C_{44} starts at 98.1 GPa ($x=0.0$), decreasing to 81.7 GPa ($x=0.6$) and increasing to 89.4 GPa ($x=1.0$). C_{55}, on the other hand, decreases from 98.1 GPa ($x=0.0$) to 70.0 GPa ($x=0.6$), while C_{66} has a minimum at $x=0.8$ (60.8 GPa). C_{12}, by the way, varies from 82.4 GPa ($x=0.0$) down to 69.6 GPa ($x=0.4$), and then up to 89.0 GPa ($x=1.0$). C_{13} (C_{23}) oscillates, with a minimum value of 73.5 (80.7) GPa at $x=0.6$ ($x=0.2$), and maximum value of 105 (90.6) GPa at $x=1.0$ ($x=0.4$). The Young modulus along the x direction (Fig. 5, bottom) is maximum for the $x=0.6$ alloy (223 GPa) and minimum for $x=1.0$ (183 GPa), while Y_y has a maximum of 214.9 GPa ($x=0.2$) and minimum of 198 GPa ($x=1.0$). Finally, Y_z has its largest value (219 GPa) for $x=0.6$, and its smallest value (180.4 GPa) for $x=1.0$.

3.2. Band structure, density of states and effective masses

In Fig. 6, we show how the Kohm–Sham minimum energy gap vary as a function of x. Using the LDA approach, the minimum energy gap increases (from 1.51 eV to 2.61 eV) as one switches from $x=0.0$ to $x=1.0$. The transition is practically linear between $x=0.2$ and $x=1.0$, with a small but noticeable change of inclination if we draw an imaginary line between the $x=0.0$ and $x=0.2$ energy gaps. The GGA gaps, on the other hand, are always smaller than LDA values, ranging from 0.74 eV ($x=0.0$) to 1.97 eV ($x=1.0$), their variation with x resembling closely the LDA data after a rigid energy shift (the difference between the LDA and GGA values is of about 0.71 eV with a standard deviation of only 0.05 eV). If one compares the calculations with the experimental band gaps presented by Mizoguchi et al. [2] for $BaSnO_3$ (3.1 eV) and $SrSnO_3$ (4.1 eV), it is very clear that the DFT gaps grossly underestimate the band gaps (by about 1.6 eV for LDA and 2.3 eV for GGA; as usual, DFT does not provide accurate gaps), but the gap variation trend is well described, with the gap difference between $x=0.0$ and $x=1.0$ being of 1.1 eV (1.2 eV) in the LDA (GGA) calculations in comparison with 1.0 eV for the experimental data. In Table 3 we describe in more detail each main band gap.

Figs. 7 and 8 show the GGA electronic band structures for the $Sr_xBa_{1-x}SnO_3$ alloys in an energy range comprising the top of the valence band (VB) and the bottom of the conduction band (CB). The Fermi level, defined here as the energy of the highest occupied state at 0 K, was gauged to be zero in all plots. LDA and GGA band structures look similar, except by a rigid energy shift, so we will present here only the GGA band structures. $BaSnO_3$ (Fig. 7(a)) has an indirect band gap of 0.74 eV between the R point in the valence band and the Γ point in conduction band. For cubic $Sr_{0.2}Ba_{0.8}SnO_3$, one can see (Fig. 7(b)) that the valence band maximum is also at the R point in reciprocal space, and the conduction band minimum appears at the Γ point, this crystal being an indirect band gap material. At the bottom of the conduction band the PDOS is relatively small due to the few electrons supported by s levels, increasing for energies above 2 eV due to contributions from $Sr_{0.2}Ba_{0.8}$-s states. A secondary indirect band gap of 0.81 eV appears between the M point in VB and the Γ point in CB, while the $\Gamma \rightarrow \Gamma$ direct gap is 1.43 eV. The top of the valence band has a strong p character with PDOS peaks at about

Table 2
Internal atomic coordinates for $Sr_xBa_{1-x}SnO_3$ series, with $x=0.2, 0.4, 0.6, 0.8$, according with the LDA and GGA calculations together with experimental (Exp.) values from Ref. [4]. The internal coordinates (u, v, w) are measured relative to the a, b and c lattice parameters of the unit cell, respectively.

Internal atomic coordinate	Atoms																			
	Ba			$Sr_{0.2}Ba_{0.8}$			$Sr_{0.4}Ba_{0.6}$			$Sr_{0.6}Ba_{0.4}$			$Sr_{0.8}Ba_{0.2}$			Sr		
	LDA	GGA	Exp.	LDA	GGA	Exp.	LDA	GGA	Exp.	LDA	GGA	Exp.	LDA	GGA	Exp.	LDA	GGA	Exp.
u	0.5	0.5	0.5	0.5	0.5	0.5	0.0	0.0	0.0	0.0	0.0	0.0	−0.002067	−0.002714	−0.0000 (8)	−0.005373	−0.005262	−0.0062 (5)
v	0.5	0.5	0.5	0.5	0.5	0.5	0.5	0.5	0.5	0.25	0.25	0.25	0.010304	0.010397	0.0109 (4)	0.025823	0.025435	0.0193 (2)
w	0.5	0.5	0.5	0.5	0.5	0.5	0.25	0.25	0.25	0.001348	−0.001419	0.0025 (6)	0.25	0.25	0.25	0.25	0.25	0.25
	Sn			Sn			Sn			Sn			Sn			Sn		
u	0.0	0.0	0.0	0.0	0.0	0.0	0.0	0.0	0.0	0.0	0.0	0.0	0.0	0.0	0.0	0.0	0.0	0.0
v	0.0	0.0	0.0	0.0	0.0	0.0	0.0	0.0	0.0	0.0	0.0	0.0	0.5	0.5	0.5	0.5	0.5	0.5
w	0.0	0.0	0.0	0.0	0.0	0.0	0.0	0.0	0.0	0.5	0.5	0.5	0.0	0.0	0.0	0.0	0.0	0.0
	O			O			O1			O1			O1			O1		
u	0.5	0.5	0.5	0.5	0.5	0.5	0.0	0.0	0.0	0.5	0.5	0.5	0.049926	0.053848	0.0487 (5)	0.064492	0.065496	0.0601 (4))
v	0.0	0.0	0.0	0.0	0.0	0.0	0.0	0.0	0.0	0.25	0.25	0.25	0.496254	0.495851	0.4921 (7)	0.488026	0.486904	0.4921 (2)
w	0.0	0.0	0.0	0.0	0.0	0.0	0.25	0.25	0.25	0.041595	0.041460	0.0406 (4)	0.25	0.25	0.25	0.25	0.25	0.25
							O2			O2			O2			O2		
u							0.266	0.266	0.265	0.25	0.25	0.25	0.733233	0.734017	0.7316 (4)	0.719072	0.718411	0.7184 (2)
v							0.766	0.766	0.765	0.021376	0.021645	0.0227 (2)	0.266954	0.265966	0.2720 (4)	0.280960	0.281227	0.2802 (2)
w							0.0	0.0	0.0	0.75	0.75	0.75	0.026557	0.028349	0.0301 (2)	0.034211	0.034440	0.0325 (2)

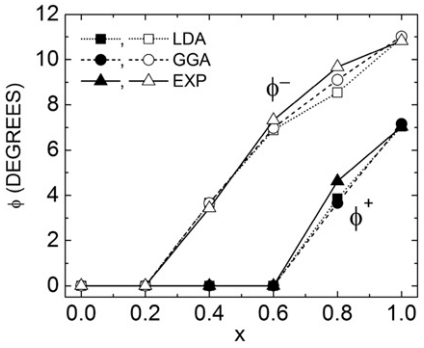

Fig. 4. Variation of the in-phase and out-of-phase tilting angles with x: DFT calculations and experiment.

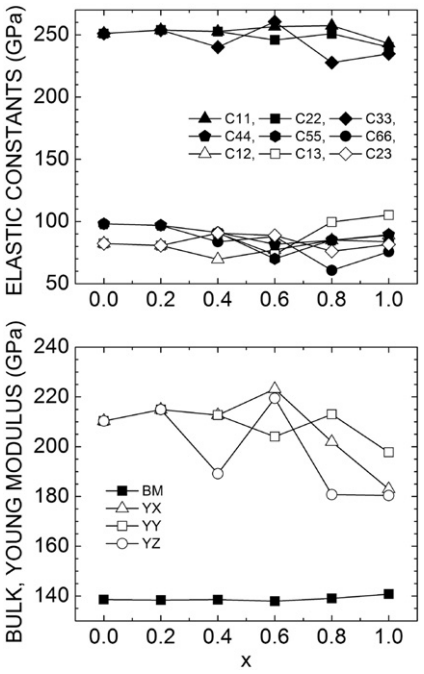

Fig. 5. Elastic constants of the $Sr_xBa_{1-x}SnO_3$ alloys calculated using the GGA-PBE functional.

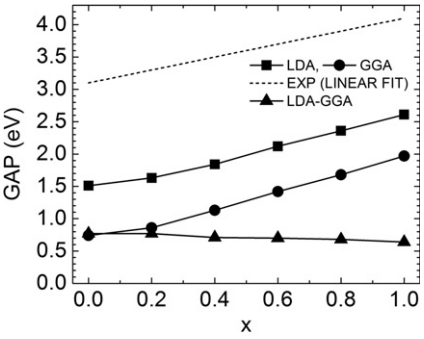

Fig. 6. Kohn-Sham minimum band gaps for $Sr_xBa_{1-x}SnO_3$. A linear fit is performed for the experimental data presented by Mizoguchi et al. [2].

−0.5 eV and −1.5 eV (as for $BaSnO_3$), while d contributions are significant only for energies above 5 eV.

In the case of $Sr_{0.4}Ba_{0.6}SnO_3$ (Fig. 7(c)), we observe a more complex electronic band structure in comparison with $x=0.0$ and $x=0.2$ due to the tetragonal crystalline structure and largest unit cell size for this alloy. The valence band maximum is at the Γ point, but with very close maxima at the M and Z points. The CB

minimum is also at Γ, with a secondary CB minimum between the X and Z points. The $\Gamma \rightarrow \Gamma$ gap is predicted to be 1.13 eV, while the $\Gamma \rightarrow$ Z gap is 2.90 eV (there is a band curve from A to Z for which the Z point looks like a minimum). Notwithstanding the differences of scale, the PDOS for $x=0.4$ is qualitatively similar to the $x=0.0,0.2$ corresponding plots, with p-like uppermost valence bands exhibiting peaks at -0.7 eV and -1.7 eV, the first being more pronounced.

Looking now to Fig. 8, one can see the band structures for the three orthorhombic unit cells corresponding to $x=0.6$ (a), 0.8 (b), and 1.0 (c), which can be compared directly (the high symmetry points are the same for all three crystals). In the $x=0.6$ and $x=0.8$ cases, the VB maximum is at the Γ point, with very close secondary maxima at X and T for $x=0.6$ and S and Z for $x=0.8$. The CB, on the other hand, has its minimum at Γ, which leads to a direct gap of 1.42 eV. For the $x=1.0$ crystal the VB maximum moves from the Γ to the S point, but the CB minimum remains at Γ. The S $\rightarrow \Gamma$ energy gap is 1.69 eV for $x=0.8$ and 1.97 eV for $x=1.0$. The direct $\Gamma \rightarrow \Gamma$ gaps, on the other hand, are 1.68 eV ($x=0.8$) and 2.02 eV ($x=1.0$). The VB maximum at T observed for $x=0.6$ disappears completely for $x=0.8,1.0$. The VB PDOS, which has two p-like maxima for $x=0.6$, has only one maximum for $x=0.8,1.0$, while the d-like CBs are shifted upwards.

Table 3
Kohn–Sham energy gaps in eV for the main electronic transitions involving valence band (VB) maxima and conduction band (CB) minima for $Sr_xBa_{1-x}SnO_3$.

Material	Transition VB→CB	LDA	GGA
$BaSnO_3$	R→Γ	1.51	0.74
(cubic)	M→Γ	1.59	0.81
$Sr_{0.2}Ba_{0.8}SnO_3$	R→Γ	1.63	0.86
(cubic)	M→Γ	1.72	0.96
	$\Gamma \rightarrow \Gamma$	2.20	1.43
$Sr_{0.4}Ba_{0.6}SnO_3$	$\Gamma \rightarrow \Gamma$	1.84	1.13
(tetragonal)	Γ→Z	5.63	2.90
$Sr_{0.6}Ba_{0.4}SnO_3$	$\Gamma \rightarrow \Gamma$	2.12	1.42
(orthorhombic)	Γ→X	5.63	3.04
$Sr_{0.8}Ba_{0.2}SnO_3$	S→Γ	2.37	1.69
(orthorhombic)	$\Gamma \rightarrow \Gamma$	2.36	1.68
	Γ→X	4.84	4.12
	Γ→Y	4.76	4.04
$SrSnO_3$	S→Γ	2.61	1.97
(orthorhombic)	$\Gamma \rightarrow \Gamma$	2.67	2.02

The effective masses give a picture of how the charge carriers respond to external electric fields in a semiconductor. They are obtained by parabolic fitting of the electronic band curves at selected high symmetry points along special directions, as shown in references [30–34]. Table 4 summarizes the electron (m_e) and hole (m_h) effective masses obtained after the DFT-GGA computations for the $Sr_xBa_{1-x}SnO_3$ alloys investigated in this work, in free electron mass units. Both hole and electron effective masses are shown to be anisotropic, but the hole masses are in general more anisotropic than electron masses. The smallest electron effective masses are observed for the cubic structures ($x=0.0,0.2$), varying between 0.03 (Γ→R) and 0.09 (Γ→X). One can note that the conduction band minimum has very close curvatures for these alloys (the electron effective masses are the same). The hole effective masses, on the other hand, vary between 0.44 (R→Γ) and 8.71 (R→M) for $x=0.0$, and between 0.43 (R→Γ) and 7.59 (R→M) for $x=0.2$. For the tetragonal phase ($x=0.4$), we have the largest hole effective mass (12.73) along Γ→M, while the smallest one occurs along Γ→A (1.40), a variation of almost one order of magnitude. For electrons, the smallest effective mass is 0.09(Γ→A) and the largest value is 0.47(Γ→Z).

For the orthorhombic alloys with $x=0.6$, 0.8, valence band curves starting at the Γ point (VB maximum) tend to become very flat as we switch from $x=0.6$ to $x=0.8$, which indicates that the corresponding effective masses become very large and difficult to estimate. In the $x=0.6$ this occurs only for the $\Gamma \rightarrow$ X band, but for $x=0.8$ it is not feasible to evaluate hole effective masses for all directions investigated, except by Γ→U and Γ→X. For the directions where the hole effective mass can be estimated, m_h stays always between 0.4 and 0.9 free electron masses. For electrons, on the other hand, effective masses tend to increase when x increases from 0.6 to 0.8, except for the mass along the

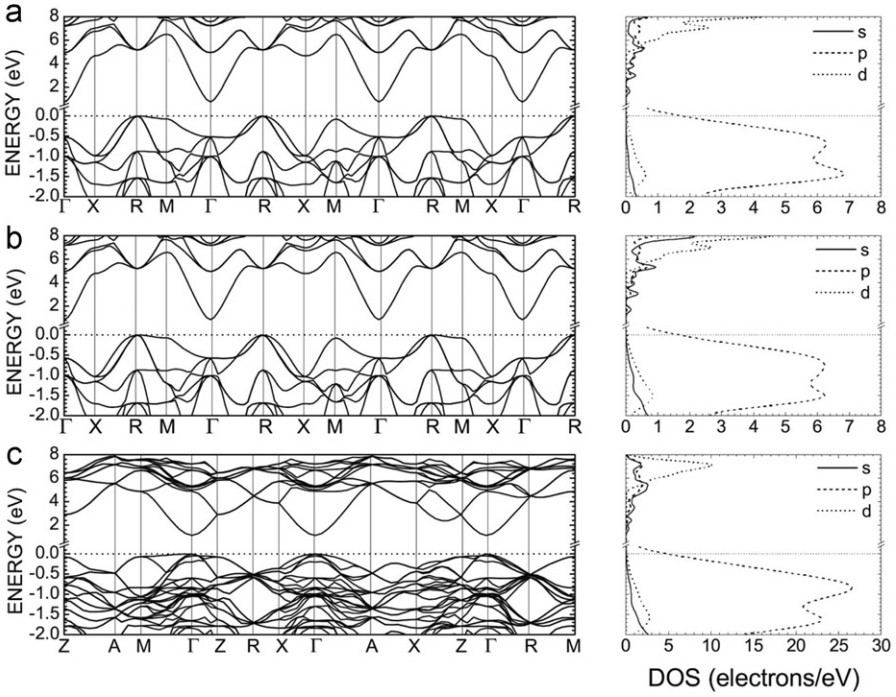

Fig. 7. Electronic band structure within the DFT-GGA approximation for (a) cubic $BaSnO_3$, (b) cubic $Sr_{0.2}Ba_{0.8}SnO_3$, and (c) tetragonal $Sr_{0.4}Ba_{0.6}SnO_3$. Partial density of states (PDOS) near the Fermi level (chosen to be zero) are also shown.

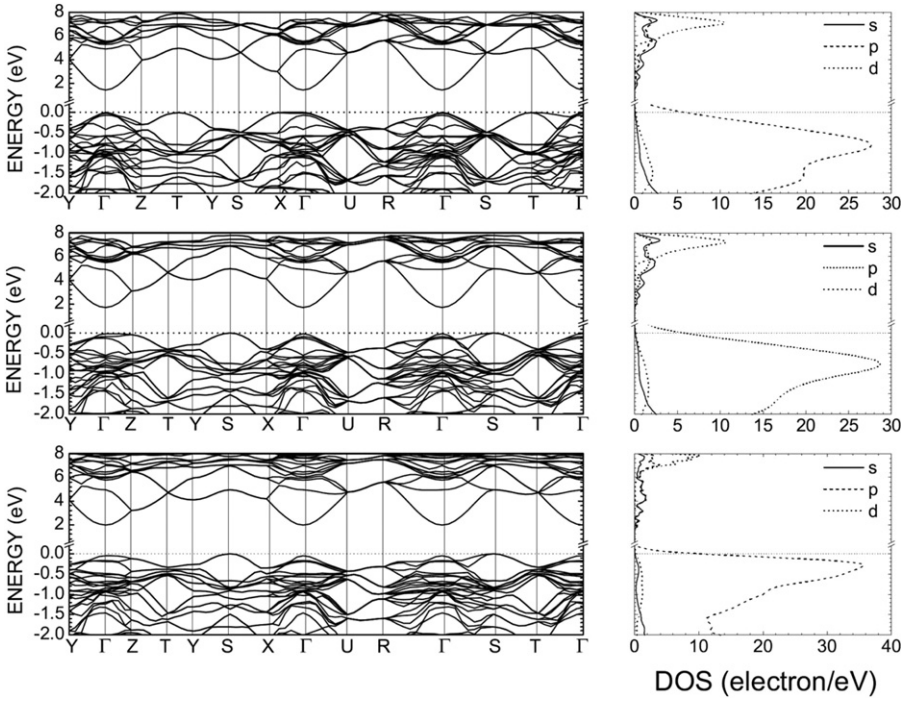

Fig. 8. Electronic band structure within the DFT-GGA approximation for (a) orthorhombic $Sr_{0.6}Ba_{0.4}SnO_3$, (b) orthorhombic $Sr_{0.8}Ba_{0.2}SnO_3$, and (c) orthorhombic $SrSnO_3$. Partial density of states (PDOS) near the Fermi level (chosen to be zero) are shown as well.

Table 4
Electron and hole effective masses for $Sr_xBa_{1-x}SnO_3$ calculated from GGA band structures. All masses are relative to the free electron mass (m_0).

Valence band	GGA	Conduction band	GGA
Cubic $BaSnO_3$			
$m_h(R\rightarrow X)$	0.92	$m_e(\Gamma\rightarrow M)$	0.05
$m_h(R\rightarrow M)$	8.71	$m_e(\Gamma\rightarrow R)$	0.03
$m_h(R\rightarrow \Gamma)$	0.44	$m_e(\Gamma\rightarrow X)$	0.09
Cubic $Sr_{0.2}Ba_{0.8}SnO_3$			
$m_h(R\rightarrow X)$	0.92	$m_e(\Gamma\rightarrow M)$	0.05
$m_h(R\rightarrow M)$	7.59	$m_e(\Gamma\rightarrow R)$	0.03
$m_h(R\rightarrow \Gamma)$	0.43	$m_e(\Gamma\rightarrow X)$	0.09
Tetragonal $Sr_{0.4}Ba_{0.6}SnO_3$			
$m_h(\Gamma\rightarrow M)$	12.73	$m_e(\Gamma\rightarrow M)$	0.12
$m_h(\Gamma\rightarrow Z)$	1.83	$m_e(\Gamma\rightarrow Z)$	0.47
$m_h(\Gamma\rightarrow X)$	3.98	$m_e(\Gamma\rightarrow X)$	0.22
$m_h(\Gamma\rightarrow A)$	1.40	$m_e(\Gamma\rightarrow A)$	0.09
$m_h(\Gamma\rightarrow R)$	1.81	$m_e(\Gamma\rightarrow R)$	0.46
Orthorhombic $Sr_{0.6}Ba_{0.4}SnO_3$			
$m_h(\Gamma\rightarrow R)$	0.43	$m_e(\Gamma\rightarrow R)$	0.12
$m_h(\Gamma\rightarrow S)$	0.76	$m_e(\Gamma\rightarrow S)$	0.19
$m_h(\Gamma\rightarrow T)$	0.42	$m_e(\Gamma\rightarrow T)$	0.15
$m_h(\Gamma\rightarrow U)$	0.95	$m_e(\Gamma\rightarrow U)$	0.21
$m_h(\Gamma\rightarrow X)$	–	$m_e(\Gamma\rightarrow X)$	0.64
$m_h(\Gamma\rightarrow Y)$	0.65	$m_e(\Gamma\rightarrow Y)$	0.26
$m_h(\Gamma\rightarrow Z)$	0.89	$m_e(\Gamma\rightarrow Z)$	0.28
Orthorhombic $Sr_{0.8}Ba_{0.2}SnO_3$			
$m_h(\Gamma\rightarrow R)$	–	$m_e(\Gamma\rightarrow R)$	0.46
$m_h(\Gamma\rightarrow S)$	–	$m_e(\Gamma\rightarrow S)$	0.51
$m_h(\Gamma\rightarrow T)$	–	$m_e(\Gamma\rightarrow T)$	2.07
$m_h(\Gamma\rightarrow U)$	0.72	$m_e(\Gamma\rightarrow U)$	0.53
$m_h(\Gamma\rightarrow X)$	0.56	$m_e(\Gamma\rightarrow X)$	0.54
$m_h(\Gamma\rightarrow Y)$	–	$m_e(\Gamma\rightarrow Y)$	2.31
$m_h(\Gamma\rightarrow Z)$	–	$m_e(\Gamma\rightarrow Z)$	1.22
Orthorhombic $SrSnO_3$			
$m_h(S\rightarrow Y)$	2.40	$m_e(\Gamma\rightarrow Y)$	0.43
$m_h(S\rightarrow X)$	1.76	$m_e(\Gamma\rightarrow Z)$	0.92
$m_{lh}(S\rightarrow \Gamma)$	0.61	$m_e(\Gamma\rightarrow X)$	0.34
$m_{hh}(S\rightarrow \Gamma)$	2.14	$m_e(\Gamma\rightarrow U)$	0.20
$m_h(S\rightarrow T)$	1.24	$m_e(\Gamma\rightarrow R)$	0.14
		$m_e(\Gamma\rightarrow S)$	0.17
		$m_e(\Gamma\rightarrow T)$	0.24

$\Gamma\rightarrow X$ direction. In particular, one can note that the $\Gamma\rightarrow Z$ electron mass starts at 0.28 for $x=0.6$, becoming 1.22 for $x=0.8$. In the $x=1.0$ case, electron effective masses decrease in comparison with their $x=0.8$ counterparts, while hole effective masses at the S point are found in the 0.6–2.4 range. Our results suggest that the $Sr_xBa_{1-x}SnO_3$ crystals can be direct ($x=0.4$, 0.6, 0.8) or indirect ($x=0.0$, 0.2, 1.0) gap semiconductors with small anisotropic electron effective masses, and large anisotropic hole masses.

4. Conclusions

In summary, we have performed first principles calculations within the density functional theory framework using LDA and GGA exchange-correlation functionals for the $Sr_xBa_{1-x}SnO_3$ alloys with $x=0.0$, 0.2, 0.4, 0.6, 0.8, 1.0, obtaining optimized geometries, elastic constants, electronic band structure and carrier effective masses. The unit cell optimizations exhibited a good agreement with the experimental results, with the LDA (GGA) optimized structures exhibiting lattice parameters 2.0% smaller (0.9% larger), at most, in comparison with neutron diffraction data. In-phase and out-of-phase tilting angles also agree well with experiment, and the elastic constants are consistent with previously published data for $BaSnO_3$. The calculated electronic band structures underestimate measured main band gaps by about 1.6 eV for the LDA, and 2.3 eV for the GGA computations. The calculated gaps vary almost linearly as a function of x for $x>0.2$, with both LDA and GGA approaches reproducing well the difference between the experimental band gaps for $BaSnO_3$ and $SrSnO_3$. The $x=0.4$, 0.6 and 0.8 alloys have direct band gaps, while $x=0.0$, 0.2, 1.0 have indirect band gaps. The PDOS reveals that the uppermost valence bands have mainly a p-like character, while the bottom of the conduction band originates mainly from s orbitals, with the presence of d levels above 5 eV. Electron and hole effective masses are anisotropic, with electron masses being lighter in comparison with hole masses. The valence band structure of the orthorhombic crystals ($x=0.6$, 0.8, 1.0) undergoes some noticeable changes as the direct

main band gap of $x=0.6$ transforms into an indirect band at $x=1.0$, with a valence band maximum at the T point ($x=0.6$) becoming a crossing of bands ($x=0.8$, 1.0) and a crossing of bands at the S point ($x=0.6$) being converted into a maximum ($x=0.8$, 1.0). A similar transformation occurs in the conduction band.

Acknowledgments

ELA, EWSC, and VNF are senior researchers from CNPq, and would like to acknowledge the financial support received during the development of this work. This work was partially financed by the Brazilian Research Agencies CAPES (Rede NanoBioTec and PROCAD), CNPq (INCT-Nano(Bio)Simes, Project no. 573925/2008-9) and FAPERN/CNPq (Pronex).

References

[1] Q.Z. Liu, H.F. Wang, F. Chen, W. Wu, J. Appl. Phys. 103 (2008) 093709.
[2] H. Mizoguchi, H.W. Eng, P.M. Woodward, Inorg. Chem. 43 (2004) 1667.
[3] Z. Lu, J. Liu, J. Tang, Y. Li, Inorg. Chem. Commun. 7 (2004) 731.
[4] E.H. Mountstevens, J.P. Attfield, S.A.T. Redfern, J. Phys.: Condens. Matter 15 (2003) 8315.
[5] H. Mizoguchi, P.M. Woodward, Chem. Mater. 16 (2004) 5233.
[6] J.M. Henriques, E.W.S. Caetano, V.N. Freire, J.A.P. da Costa, E.L. Albuquerque, J. Phys.: Condens. Matter 19 (2007) 106214.
[7] V.V. Bannikov, I.R. Shein, V.L. Kozhevnikov, A.L. Ivanovskii, J. Magn. Magn. Mater. 320 (2008) 936.
[8] I.R. Shein, V.L. Kozhevnikov, A.L. Ivanovkii, Semiconductors 40 (2006) 1261.
[9] W.F. Zhang, J. Tang, J. Ye, Chem. Phys. Lett. 418 (2006) 174.
[10] E. Moreira, J.M. Henriques, D.L. Azevedo, E.W.S. Caetano, V.N. Freire, E.L. Albuquerque, J. Solid State Chem. 184 (2011) 921.
[11] L. Bellaiche, D. Vanderbilt, Phys. Rev. B 61 (2000) 7877.
[12] B. Winkler, C.J. Pickard, V. Milman, Chem. Phys. Lett. 362 (2002) 266.
[13] M. Mikami, K. Uheda, N. Kijima, Phys. Status Solidi (a) 203 (2006) 2705.
[14] D.J. Wilson, B. Winkler, E.A. Juarez-Arellano, A. Friedrich, K. Knorr, C.J. Pickard, V. Milman, J. Phys. Chem. Sol. 69 (2008) 1861.
[15] P. Hohenberg, W. Kohn, Phys. Rev. 136 (1964) B864.
[16] W. Kohn, L.J. Sham, Phys. Rev. 140 (1965) A1133.
[17] M.D. Segall, P.L.D. Lindan, M.J. Probert, C.J. Pickard, P.J. Hasnip, S.J. Clark, M.C. Payne, J. Phys.: Condens. Matter 14 (2002) 2717.
[18] R.O. Jones, O. Gunnarsson, Rev. Mod. Phys. 61 (1989) 689.
[19] O.V. Gritsenko, P.R. Schipper, E.J. Baerends, J. Chem. Phys. 107 (1997) 5007.
[20] A. Dal Corso, A. Pasquarello, A. Baldereschi, R. Car, Phys. Rev. B 53 (1996) 1180.
[21] M. Fuchs, M. Bockstedte, E. Pehlke, M. Scheffler, Phys. Rev. B 57 (1998) 2134.
[22] D.M. Ceperley, B.J. Alder, Phys. Rev. Lett. 45 (1980) 566.
[23] J.P. Perdew, A. Zunger, Phys. Rev. B 23 (1981) 5048.
[24] J.P. Perdew, K. Burke, M. Ernzerhof, Phys. Rev. Lett. 77 (1996) 3865.
[25] J.P. Perdew, J.A. Chevary, S.H. Vosko, K.A. Jackson, M.R. Pederson, D.J. Singh, C. Fiolhais, Phys. Rev. B 46 (1992) 6671.
[26] J.S. Lin, A. Qteish, M.C. Payne, V. Heine, Phys. Rev. B 47 (1993) 4174.
[27] A.M. Rappe, K.M. Rabe, E. Kaxiras, J.D. Joannopoulos, Phys. Rev. B 41 (1990) 1227.
[28] H.J. Monkhorst, J.D. Pack, Phys. Rev. B 13 (1976) 5188.
[29] B.G. Pfrommer, M. Cote, S.G. Louie, M.L. Cohen, J. Comput. Phys. 131 (1997) 133.
[30] J.M. Henriques, E.W.S. Caetano, V.N. Freire, J.A.P. da Costa, E.L. Albuquerque, Chem. Phys. Lett. 427 (2006) 113.
[31] S.K. Medeiros, E.L. Albuquerque, F.F. Maia Jr., E.W.S. Caetano, V.N. Freire, Chem. Phys. Lett. 435 (2007) 59.
[32] J.M. Henriques, E.W.S. Caetano, V.N. Freire, J.A.P. da Costa, E.L. Albuquerque, J. Solid State Chem. 180 (2007) 974.
[33] C.A. Barboza, J.M. Henriques, E.L. Albuquerque, V.N. Freire, J.A.P. da Costa, E.W.S. Caetano, J. Phys. D: Appl. Phys. 42 (2009) 155406.
[34] C.A. Barboza, J.M. Henriques, E.L. Albuquerque, E.W.S. Caetano, V.N. Freire, J.A.P. da Costa, Chem. Phys. Lett. 480 (2009) 273.
[35] C.J. Howard, K.S. Knight, B.J. Kennedy, E.H. Kisi, J. Phys.: Condens. Matter 12 (2000) 677.
[36] B.J. Kennedy, B.A. Hunter, J.R. Hester, Phys. Rev. B 65 (2002) 224103.
[37] P.S. Beurmann, V. Thangadurai, W. Weppner, J. Solid State Chem. 174 (2003) 392.
[38] A. Bouhemadou, K. Haddadi, Solid State Sci. 12 (2010) 630.
[39] J.C. Farfán, J.A. Rodríguez, F. Fajardo, E.V. López, D.A. Landínez Téllez, J. Roa-Rojas, Physica B 404 (2009) 2720.
[40] T. Maekama, K. Kurosaki, S. Yamanaka, J. Alloys Compd. 416 (2006) 214.
[41] I.R. Shein, V.L. Kozhevnikov, A.L. Ivanovskii, Solid State Sci. 10 (2008) 217.